CrossMark

Sedimentary geochemical evidence of historical tsunamis in the Eastern Mediterranean from Ölüdeniz Lagoon, SW Turkey

Ulaş Avşar

Abstract In the Eastern Mediterranean and southern Aegean seas, historical records indicate there were 17 tsunamis in the last 2500 years with intensities > 6 on a 12-point tsunami intensity scale. Regional geologic records of past tsunamis, however, are not sufficiently well-documented to assess tsunami hazards. This study presents geochemical evidence of historic tsunamis in the Eastern Mediterranean for the last 700 years, detected in the sedimentary sequence of Ölüdeniz Lagoon, SW Turkey. Sediment chronology was established by ^{137}Cs and ^{210}Pb dating, and regional chronostratigraphic correlation reveals that three events observed within the sequence correlate temporally with the AD 1303, 1609, and 1741 tsunamis in the region. The sediment anomalies (tsunami deposits) appear as reddish-brown intercalations within yellowish-brown background sediments of the lagoon, and are enriched in K, Ti, Fe and Zn, but depleted in Ca. This kind of geochemical fingerprint is attributed to a sudden increase in the input of terrigenous sediment to the lagoon, which was swept from Ölüdeniz beach and the sand spit of the lagoon by marine overwash during tsunamis. If the stratigraphic thickness and magnitude of the geochemical anomalies are assumed to be a proxy for tsunami intensity, then the AD 1609 event was stronger in the Ölüdeniz region than the AD 1303 and 1741 tsunamis.

Keywords Paleotsunami · XRF analysis · ITRAX core scanner · Chronostratigraphic correlation

Introduction

Among many tsunamis during the twentieth and twenty-first centuries, the Mw 9.1 Sumatra (Indonesia) offshore earthquake on 26 December 2004 triggered the most devastating tsunami in recorded history, killing 230,000 people (ITIC 2018). Seven years later, on 11 March 2011, the Mw 9.0 Tohoku (Japan) offshore megathrust earthquake triggered another tsunami, which caused 15,270 deaths and left 8500 people missing as of May 2011 (ITIC 2018). These two events are reminders that tsunamis are serious threats to human lives and infrastructure, and that tsunami hazard assessment studies, especially paleo-tsunami investigations, are necessary to reveal tsunami recurrence frequency. During the 2004 and 2011 tsunamis, run-up heights at coastal sites reached 30 m, inundating sites up to 20 km inland (Borrero et al. 2006; Mori et al. 2011).

U. Avşar (✉)
Department of Geological Engineering, Middle East Technical University, 06800 Ankara, Turkey
e-mail: uavsar@metu.edu.tr

U. Avşar
Physical Science and Engineering Division (PSE), King Abdullah University of Science and Technology (KAUST), Thuwal, Saudi Arabia

Springer

In addition to the casualties, the infrastructure loss caused by the Tohoku and Sumatra tsunamis were estimated to be about US $200–300 and $10 billion, respectively (ITIC 2018). The economic loss was caused by physical damage to infrastructure, as well as boats/ships within ports, harbors and marinas. The 2004 Sumatra and 2011 Tohoku tsunamis also deposited sediment up to 4 m thick in the Kirinda (Sri Lanka) and Crescent City (California) harbors, respectively (Goto et al. 2010; Wilson et al. 2012). Another tsunami-induced hazard is contamination of groundwater and agricultural soils, caused by seawater inundation, which can reduce crop yields during post-tsunami periods. Experience from the 2004 Sumatra tsunami revealed that soils recover to pre-tsunami levels within 6 months to a year; however, groundwater models suggest that contamination can persist for 10–15 years (Chandrasekharan et al. 2008; McLeod et al. 2010). Tsunamis can also severely affect coastal ecosystems, from which we obtain a substantial proportion of total seafood. High-energy waves alter the nursery areas for fish and benthic organisms, as well as the nutrient balance in the water. These impacts can affect the entire food web in coastal ecosystems for decades (Fuhrman et al. 2015).

The above-mentioned damages caused by tsunamis add urgency to tsunami hazard assessment studies. The goal is to mitigate the devastating consequences of tsunamis, as has been done successfully in probabilistic seismic hazard assessment (PSHA) analyses. Compared to the amount of seismological data used in PSHA analyses, however, the number of known tsunamis is relatively low, which prevents developing standard and low-uncertainty statistical approaches like those used in PSHA analyses (Papadopoulos et al. 2014). In addition to instrumentally recorded datasets, PSHAs use historical and geological records of past earthquakes to make reliable estimates of long-term patterns of seismicity. Similarly, tsunami hazard assessments require information from historical and geological records. The lengths and quality of historical tsunami records from around the world differ substantially. For most of the world, historical records do not extend back in time sufficiently to evaluate the recurrence of tsunamis. Besides, even if the historical records for a region are long enough, they can be incomplete for multiple reasons, e.g. (1) if a tsunami affected an uninhabited area, it might not be reported, (2) records might have been lost because of political

instability during or after the tsunami (Hadler et al. 2012). Thus, geological archives in coastal and near-shore depositional environments are crucial to assess reliably the recurrence frequency of tsunamis.

Coastal depositional environments, where sedimentary traces of tsunamis are potentially recorded, include mainly lagoons (Kelsey et al. 2005; Donato et al. 2009; Peterson et al. 2011; May et al. 2012a; Jackson et al. 2014), tidal wetlands and enclosed water bodies (Sawai et al. 2009; Dura et al. 2015; Kempf et al. 2015, 2017; Baranes et al. 2016), back-barrier wetlands (Clark et al. 2011; Peterson et al. 2011; May et al. 2012b), fluvial plains (Vött et al. 2011; Alpar et al. 2012; Papadopoulos et al. 2012; Kitamura et al. 2013), and the near-shore shelf (van den Bergh et al. 2003; Goodman-Tchernov et al. 2009; Gutiérrez-Mas et al. 2009; Smedile et al. 2011; Tyuleneva et al. 2018). When high-energy tsunami waves reach the coast, they mobilize substantial amounts of material from areas near the shoreline and transport it inland during the inflow. The mobilized material, composed of grain sizes that can vary from clay to boulders, is deposited in terrestrial lowlands as inflow deposits, generally thinning and fining inland. Among coastal depositional environments, sediment sequences of aquatic environments, i.e. lagoons and coastal lakes, provide relatively complete and longer paleo-tsunami chronologies (Nanayama et al. 2003; Kelsey et al. 2005; Jackson et al. 2014; Kempf et al. 2017), and therefore can contribute to tsunami hazard assessment.

Paleo-tsunami deposits appear as intercalations within sedimentary sequences of coastal depositional environments and are generally recognized by investigating physical, geochemical and microbiological content of sediments (Röbke and Vött 2017). The most common method applied is grain-size-distribution analysis, which provides valuable information about the hydrodynamic conditions during deposition. For instance, coarser-grained intercalations (generally sandy) and fining-upward sequences reflect a decrease in the turbulence of the flow during inundation (Nanayama et al. 2007; Smedile et al. 2011; Razjigaeva et al. 2014; Dura et al. 2015; Graehl et al. 2015). Microbiological analyses of diatom (Kelsey et al. 2005; Goff et al. 2011; Dura et al. 2015; Graehl et al. 2015), foraminifera (Mamo et al. 2009; Bertrand et al. 2011; Pilarczyk and Reinhardt 2012; Mathes-Schmidt et al. 2013; Willershäuser et al. 2015; Fischer et al. 2016) and ostracod (Ruiz et al. 2010; Mischke et al.

2012) assemblages in tsunami deposits is another common method used to reveal the marine origin of deposits intercalated within coastal, land-derived sediment sequences. Paleo-tsunami deposits can also be detected by their geochemical signature within sediment sequences. A number of studies utilized conventional XRF analysis to identify chemical fingerprints of marine origin in tsunami deposits. In general, tsunami deposits are enriched in elements like sodium, sulphur, chlorine, calcium, strontium and magnesium (Vött et al. 2009a; Chagué-Goff 2010; Chagué-Goff et al. 2011, 2017; Ramírez-Herrera et al. 2012; Mathes-Schmidt et al. 2013; Baranes et al. 2016).

Sedimentary evidence of extreme wave events (EWE) has been detected within numerous onland, coastal sediment sequences. The main debate in paleo-tsunami research revolves around whether detected EWE deposits are of tsunami or storm surge origin. With regard to the "storm versus tsunami" debate, paleo-tsunami investigations conducted in the Mediterranean region have advantages over those conducted along the shores of the Pacific and Indian Oceans. Vött et al. (2018) stated that Mediterranean tsunamis comprised 73–98% of all EWE for the period 1902–2017. These statistics suggest that the possibility that storm surges in the Mediterranean produce geological traces similar to those caused by tsunamis can be assumed to be insignificant. This makes coastal depositional environments around the Mediterranean Sea ideal targets to conduct paleo-tsunami investigations. In this study, I present geochemical evidence of historical tsunamis in the eastern Mediterranean, which were identified within the fine-grained sedimentary sequence of Ölüdeniz Lagoon, SW Turkey, by micro-XRF scanning of three approximately 1-m-long sediment cores.

Study area

In the Mediterranean Sea (Fig. 1), 37 tsunamis having intensities > 6 within a 12-point tsunami intensity scale (Papadopoulos and Imamura 2001), were reliably documented for the interval of the last 2500 years (Papadopoulos et al. 2014). Among these historically recorded events, 17 tsunamis directly affected the coasts of the southern Aegean and eastern Mediterranean Seas, yielding a mean tsunami recurrence of

∼ 150 years. The active tectonics of the region is mainly a consequence of the relative motions among the African, Arabian and Anatolian plates (Fig. 1a). Subduction of the African plate under the Anatolian plate gave rise to the Hellenic and Cyprus arcs, with the Pliny-Strabo Fault Zone sinistrally offsetting the arcs. In addition, the Cyclades Archipelago in the southern Aegean appears as a result of back-arc extension and related volcanism caused by the Hellenic subduction. Relative motion between the African and Arabian plates results in sinistral motion along the Dead Sea Transform Fault (Barka and Reilinger 1997). The potential of these neotectonic structures to trigger tsunamis is "high" for the eastern Hellenic Arc, "intermediate" for the Cyclades and the Dead Sea Fault, and "low" for the Cyprus Arc (Yolsal et al. 2007; Papadopoulos et al. 2014).

Among the historical tsunamis (Fig. 1a), the ones in 1613 ± 13 BC (Thera), AD 365 (SW Crete), AD 1303 (Eastern Crete), AD 1650 (Cyclades) and AD 1956 (Cyclades), were the most disastrous, having intensities of 9–10 (Papadopoulos et al. 2014). In contrast to the extensive historical tsunami record, the geologic record of paleo-tsunamis in the region (yellow diamonds in Fig. 1a) are far from providing a paleo-tsunami chronology that can contribute to tsunami hazard assessment. The geologic records in Didim and Fethiye (Di and F; Minoura et al. 2000), Palaikastro (EC; Bruins et al. 2008) are records of a single event that was the tsunami triggered by the Minoan eruption of Santorini around 1613 ± 13 BC. The studies in Alexandria (Al; Stanley and Bernasconi 2006), Ashkelon (As; Hoffmann et al. 2018), Crete (SWC; Werner et al. 2018), Marsa-Matrouh (Ma; Shah-Hosseini et al. 2016), Cyprus (Cy1 and Cy2; Whelan and Kelletat 2002), Thera (Th; Dominey-Howes et al. 2000b), Livadia (Li; Dominey-Howes et al. 2000a) and Silifke (Si; Öğretmen et al. 2015) also report single events, which occurred in 5600 BP, 400 BC, AD 365, AD 1303, AD 1500–1800, AD 1650, AD 1953, and AD 1956, respectively. There are only four locations where multiple paleo-tsunamis were reported: in Western Crete (WC), Lebanon (Le), Caesarea (Ca) and Dalaman (D, SW Turkey). The traces of four paleo-tsunamis in 5660 BP, AD 66, AD 365, and AD 1500 were reported in western Crete (WC; Pirazzoli et al. 1992; Scheffers and Scheffers 2007), and probably had more effect in the Ionian Sea. Within the near-shore shelf sediments close to the
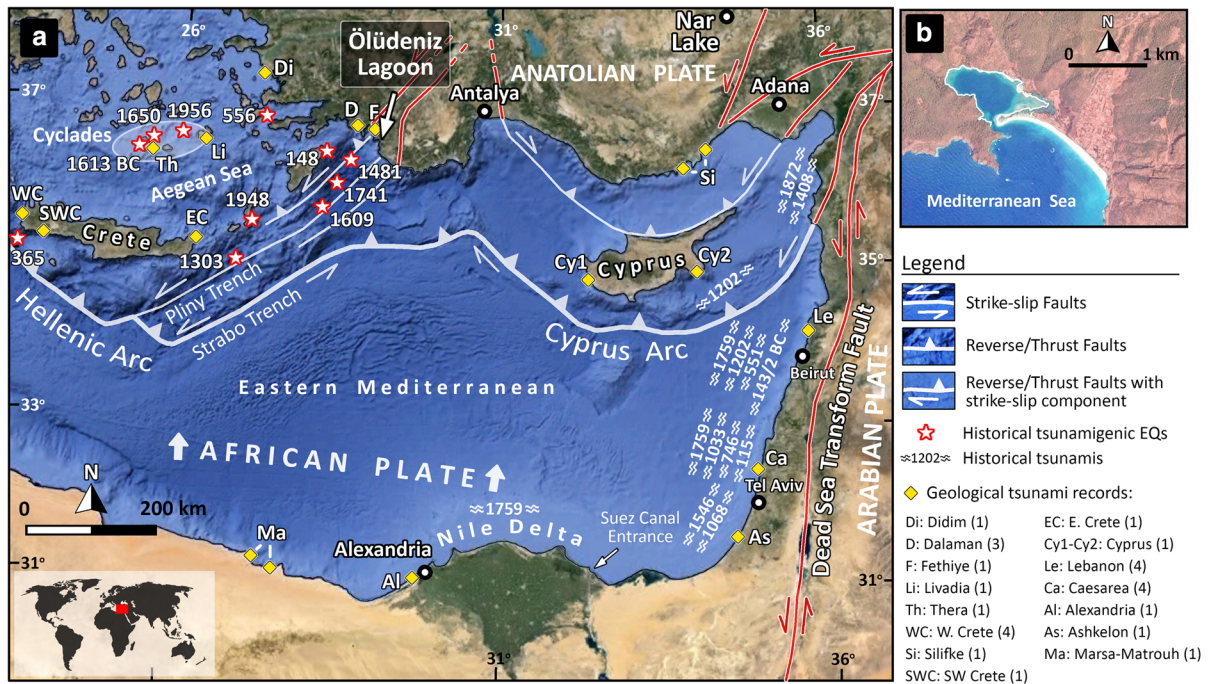
Fig. 1 a Tectonic setting in the Eastern Mediterranean (simplified from Barka and Reilinger 1997), the dates and epicentres of historical tsunamigenic earthquakes in the eastern Hellenic Arc and the Cyclades (stars) (Papadopoulos et al. 2014), and the historical tsunamis along the eastern coasts of the Mediterranean Sea (e.g. ~ 1759) mainly caused by earthquakes on the Cyprus Arc and the Dead Sea Transform Fault (Salamon et al. 2007). The locations of geological paleotsunami records in the region are shown by yellow diamonds. The numbers in parentheses next to the names of the geological paleotsunami records in the legend stand for the number of detected paleotsunamis at that location. **b** Close-up view of Ölüdeniz Lagoon. Elevations higher than 5 m a.s.l. are overlain by transparent red polygon. (Color figure online)

ancient city of Caesarea (Ca in Fig. 1a), Goodman-Tchernov et al. (2009) and Tyuleneva et al. (2018) report tsunamis in the 4th millennium BC, 1630–1550 BC (Santorini Tsunami), AD 115 and AD 551. In Lebanon, megablocks left by extreme waves were dated to 3639–3489 BC, AD 1436–1511, AD 1528–1673 and AD 1690–1950 (Le; Morhange et al. 2006). In SW Turkey, sediment records of tsunamigenic earthquakes on the eastern Hellenic Arc in AD 1303, 1481 and 1741 were found in the sequence of the Dalaman alluvial plain (Alpar et al. 2012; Papadopoulos et al. 2012).

Ölüdeniz Lagoon, which is located in SW Turkey (Fig. 1a, b), is an ideal place along the coast of the eastern Mediterranean to investigate sedimentary traces of past tsunamis. A well-developed, approximately 500-m-long sand spit, the elevation of which does not exceed 5 m a.s.l. (Fig. 2), isolates the lagoon from the sea and hence provides a calm depositional environment for fine-grained sediments. Furthermore, the flat nature of the sand spit enables overwash during

tsunamis, which would leave traces within the background sedimentation of the lagoon. The water depth in the lagoon reaches a maximum of 38 m (Fig. 2a). The lithology in the catchment that provides sediment to the lagoon and the associated near-shore environment is dominated by limestone and carbonaceous clastics (Fig. 2b).

Materials and methods

The bathymetry of Ölüdeniz Lagoon was developed using a high-resolution depth-sounding grid (~ 50-m spacing) obtained from a boat equipped with a sonar-mounted Global Positioning System (GPS) device (Garmin GPSmap 421 s). Three gravity cores with a diameter of 7.5 cm were collected from the lagoon in May 2014; OLD-14-1 (84 cm long; 688,970E, 4,047,220N), OLD-14-2 (99 cm long, 688,810E, 4,047,310N) and OLD-14-3 (102 cm long; 688,820E, 4,047,210N) (Fig. 2a). Sediment
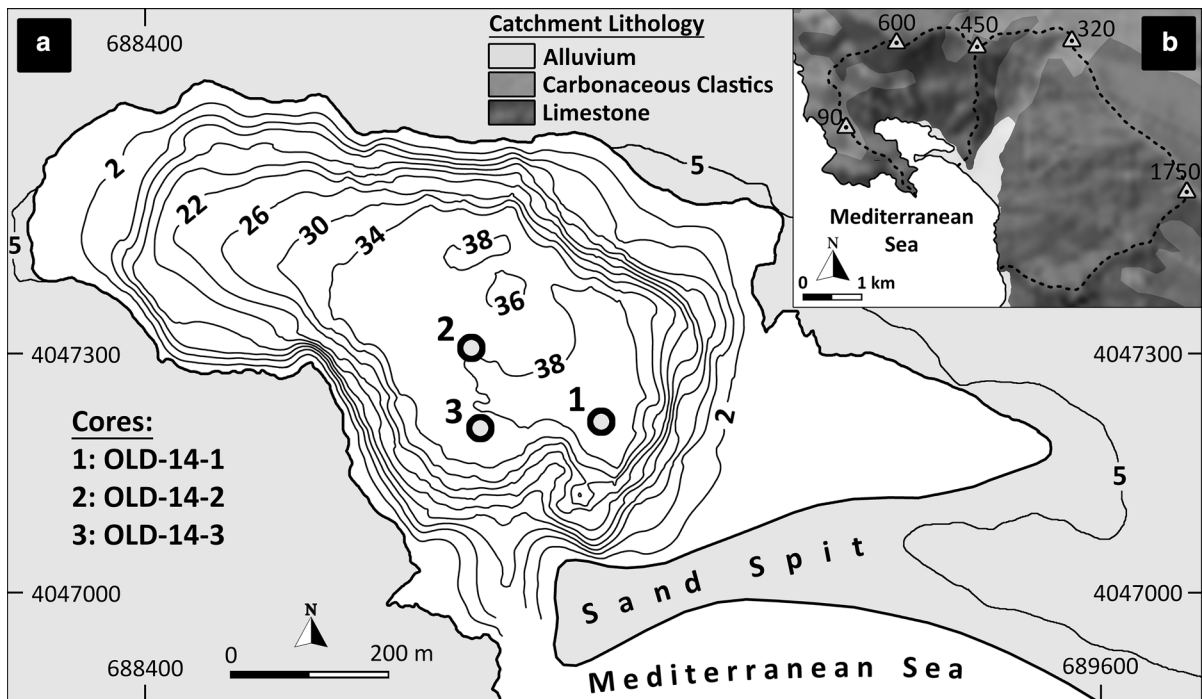
Fig. 2 **a** Bathymetry of Ölüdeniz Lagoon and sediment core locations. Note the 5-m elevation contour around the lagoon. **b** Lithology within the catchment of the lagoon and the associated near-shore environment. Numbers next to the triangles denote the elevations

chronology in the upper part of OLD-14-2 was developed from ^{137}Cs and excess ^{210}Pb (^{210}Pb$_{xs}$) activity measured on 12 samples (1-cm-thick), obtained using a low-background, high-efficiency well-type gamma spectrometer at the University of Bordeaux. Immediately after splitting the cores, they were sent to GEOPOLAR Laboratory at the University of Bremen for ITRAX micro-X-ray fluorescence (µXRF) scanning, and to obtain optical and radiographic images. ITRAX scanning was done by Mo-tube, with an exposure time of 10 s every 1 mm. The XRF data for each element was standardized (Eq. 1) to create comparable units between different elements and cores. To obtain standardized plots, the means (µ) and standard deviations (σ) were calculated for each element profile. Subtracting the mean value from each data value (x), and then dividing it by the standard deviation of the corresponding elemental profile, yielded a new re-scaled element profile with a mean value of "0" and standard deviation of "1." In this way, the semi-quantitative datasets provided by the ITRAX scanner were converted into datasets having similar and comparable scales.

$$z = \frac{x - \mu}{\sigma} \tag{1}$$

where x = data value, µ = mean, and σ = standard deviation.

Because no datable organic plant remains were found in the sediments, radiocarbon dating was not possible. Hence, the mean sedimentation rate determined for the top ∼ 1/3 of the sequence by ^{137}Cs–^{210}Pb$_{xs}$ was assumed to be the same for the lower parts of the sequence. This assumption was tested by regional time-stratigraphic correlation of the Ölüdeniz record with the varve-based δ^{18}O record from Nar Lake (Fig. 1a) (Jones et al. 2006), which was successfully applied to another Anatolian lake by Avşar et al. (2014).

Results

Standardized profiles of 16 elements obtained by ITRAX XRF scanning of the three cores from Ölüdeniz Lagoon are presented in Fig. 3. The sediment sequence in the three cores is composed mainly of yellowish-brown sandy silt. The sequences look
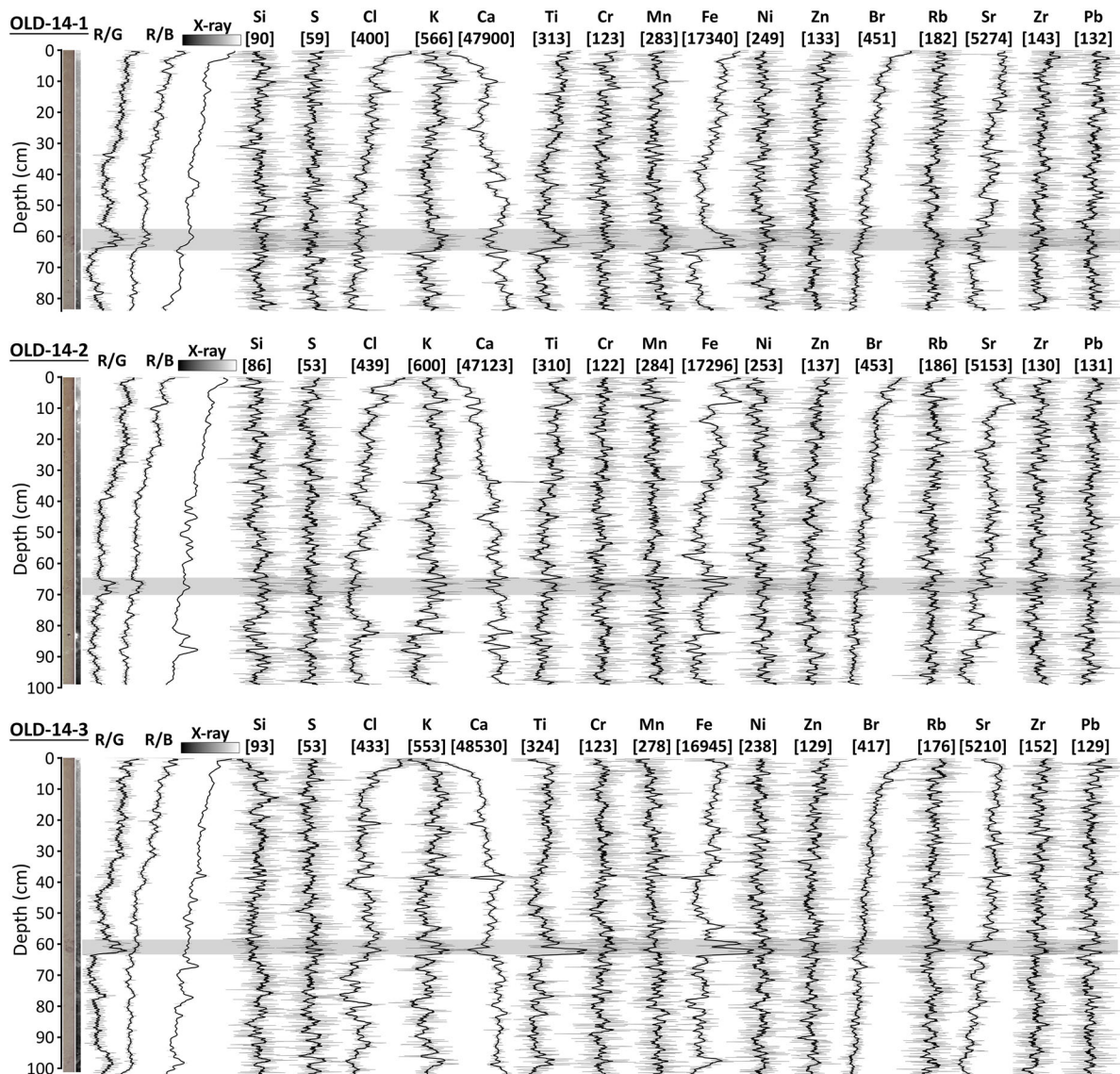
Fig. 3 Optical and radiographic images, and the micro-XRF scanning results from the cores collected in Ölüdeniz Lagoon. Red/Green (R/G) and Red/Blue (R/B) profiles are presented to visualize the redness changes along the optical images of the cores, and the X-ray grayscale profiles to visualize the darkness along the radiographic images. Visually, a reddish brown intercalation (gray bar) is prominent especially in the R/G profiles. The intercalation is also characterized by anomalies in the K, Ti and Fe profiles. The raw element profiles (1-mm resolution) are presented in gray, and overlain by a 9-point moving average (black lines). Numbers in brackets are average counts for each element

relatively homogenous, but display slight fluctuations along the elemental profiles. There is, however, a visually apparent reddish-brown, 3–5-cm-thick intercalation in all three cores (gray bars in Fig. 3). To quantify the relative changes in redness along the sediment sequences, red values were divided by green and blue values for each pixel of the optical images, and plotted along the cores. The redness of the intercalation appears as an anomaly along R/G and R/B profiles (Fig. 3). The intercalation is also chemically characterized by anomalies in the K, Ti and Fe profiles. On the other hand, the grayscale plots of the radiographic images show no significant change caused by the intercalation.

The $^{210}Pb_{xs}$ activity reveals a profile with three distinct decay trends (Fig. 4a), having r^2

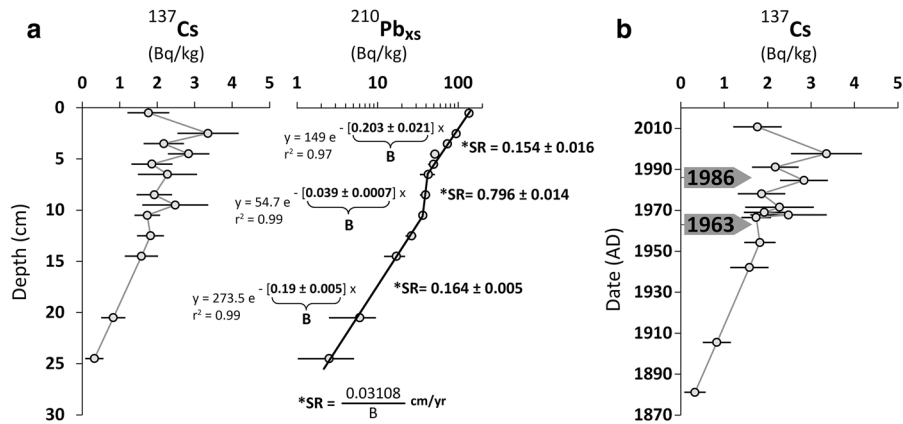**Fig. 4** **a** Plots of ^{137}Cs and [210]Pb$_{xs}$ activity in the top 25 cm of the OLD-14-2 core. The ^{137}Cs profile does not display clear peaks, whereas the [210]Pb$_{xs}$ profile reveals three trends corresponding to different sedimentation rates (SR): 0.164 cm/year (25–10 cm), 0.797 cm/year (10–7 cm), and 0.153 cm/year (7–0 cm). **b** Plot of ^{137}Cs profile with respect to dates calculated from the [210]Pb$_{xs}$-derived SRs

values > 0.97. The "Constant Flux Constant Sedimentation Rate" model enables calculation of sedimentation rates by dividing 0.03108 (the ^{210}Pb decay constant) by the slope of exponential best fits ("B"s in Fig. 4a). Calculated sedimentation rates for the intervals 25–10, 10–7, and 7–0 cm are 0.164 ± 0.005, 0.796 ± 0.014 and 0.154 ± 0.016 cm/year, respectively. The ^{137}Cs profile was not very useful for dating the profile because it failed to display two distinct peaks that could be attributed to the maximum fallout in 1963 from atmospheric nuclear weapon tests and the Chernobyl reactor accident in 1986. If the ^{137}Cs profile is re-plotted based on the sedimentation rates (SRs) calculated using the [210]Pb$_{xs}$ decay profile, the 1963 peak is offset by about 4 years and there is a weak anomaly around 1986 (Fig. 4b). Presence of a peak around 1997, however, discredits this interpretation. Given that the ^{137}Cs values are very low throughout the profile (maximum = 4 Bq/kg), the small peaks around 1967 and 1986 may simply reflect measurement errors and should not be over-interpreted. Considering the high r^2 values of the best-fits along the [210]Pb$_{xs}$ decay profile, the [210]Pb$_{xs}$-based SRs seem reasonable. Hence, except the high SR from 10 to 7 cm, an SR from 0.15 to 0.17 cm/year along OLD-14-2 core seems acceptable.

Discussion

The reddish-brown intercalation in the sequence is observed more clearly in the OLD-14-1 and OLD-14-3 cores at around 60 cm (Fig. 3). The Ti and Fe anomalies associated with this intercalation, in particular, are distinct and almost unique compared to other minor fluctuations along the lengths of the cores. The sharp increase at the bottom of the anomalies and gradual decrease upwards implies a sudden change in sedimentation, i.e. a sedimentary event. Although this study does not present any grain-size distribution analysis, which is a commonly used diagnostic proxy to detect tsunami-related sedimentary event deposits, grain-size analysis should be considered within the frame of future studies to verify geochemical anomalies. Down-core extrapolation of the 0.164 ± 0.005 cm/year SR, which was obtained from the lower part of the [210]Pb$_{xs}$ profile, revealed that the reddish-brown intercalation dates to the early seventeenth century (Fig. 5a, b). This sedimentary event (E2) correlates temporally with the damaging tsunami in AD 1609, caused by an earthquake offshore of Rhodes Island, ~ 130 km southwest of Ölüdeniz Lagoon (Fig. 1). That tsunami had an intensity of 8 (in the area of Rhodes Island) on the 12-point scale of Papadopoulos and Imamura (2001) (Papadopoulos et al. 2014). A brownish tsunami layer was also reported within the sequence of Lake Voulkaria in NW Greece (Vött et al. 2006, 2009b), which was first recognized by Jahns (2005).
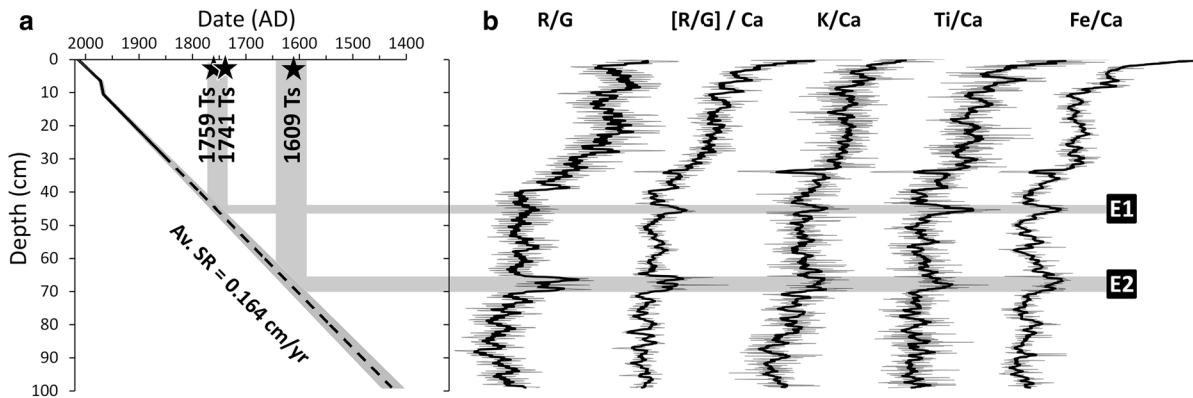
Fig. 5 **a** Age-depth model for the OLD-14-2 core. Solid line was obtained from $^{210}Pb_{xs}$ measurements, and the dashed line is the extrapolation of 0.164 cm/year SR down to the bottom of the core. The gray area surrounding the dashed line indicates the error in the age-depth model. **b** Plot of R/G values and micro-XRF data for OLD-14-2. The reddish-brown intercalation presented in Fig. 3 is dated to the beginning of the seventeenth century (E2), when a historically documented strong tsunamigenic earthquake took place offshore Rhodes Island, in AD 1609. Another similar anomaly (E1) corresponds temporally to a tsunami that occurred in AD 1741. XRF data imply depletion in Ca, enrichment in K–Ti–Fe, or both, as a consequence of the tsunamis

Because ITRAX scanning is done directly on the sediment surface along cores, scanning results bear traces of physical properties of sediments as well, such as water and organic matter content, and hence are semi-quantitative. To reduce the effects of sediment physical properties, element ratios can be used to better evaluate relative changes in element concentrations. In Fig. 5b, the R/G, K, Ti and Fe profiles are normalized to Ca. This normalization reveals the anomalies related to E2. Accordingly, it can be said that the geochemical trace of the AD 1609 tsunami is characterized by enrichment in K, Ti, Fe, depletion in Ca, or both. An analogous sedimentary event is also seen around the mid-eighteenth century (E1 in Fig. 5b). This event can be attributed to the AD 1741 tsunami, which had an intensity of 8 in the area of Rhodes Island (Papadopoulos et al. 2014). Another tsunami hit the Nile Delta and the easternmost coast of the Mediterranean Sea in AD 1759 (Salamon et al. 2007); there is, however, no historical record that it affected the northern coast of the eastern Mediterranean.

In paleolimnological studies, multiple cores are crucial to evaluate the basin-wide extent of sedimentary events, and rule out local and micro-sedimentary processes like sediment focusing, post-depositional diagenesis and coring disturbances. In Ölüdeniz Lagoon, inter-core stratigraphic correlation was achieved by correlating the (R/G)/Ca, K/Ca, Ti/Ca

and Fe/Ca profiles of OLD-14-1 and OLD-14-3 with those of OLD-14-2 (Fig. 6). Age-depth models for OLD-14-1 and OLD-14-3 that resulted from the correlation with OLD-14-2 do not deviate much from each other (Fig. 6a), i.e. unreasonable SR assumptions were not made. In Fig. 6b, it can be seen that E1 and E2 correlate in all three cores. Since OLD-14-3 covers a longer time period, it reveals one more event (E3) that is analogous with E1 and E2. Accordingly, E3 occurred at the beginning of the fourteenth century, implying that it was caused by the AD 1303 tsunami. This tsunami had an intensity of 10 in the eastern part of Crete (Papadopoulos et al. 2014), approximately 300 km southwest of Ölüdeniz Lagoon (Fig. 1a).

To obtain an overall view of the tsunami-related proxies presented in Fig. 6b, the data from the three cores were superimposed, and their average profiles are presented in Fig. 7. Anomalies related to the AD 1303, 1609 and 1741 (or 1759) tsunamis are highly consistent along Ca-normalized profiles, especially along the Ti/Ca profile. Normalization of profiles for elements like Ti, Fe, K and Zn, by Ca, is used to evaluate changes in the balance between terrestrial clastic deposition and deposition of biologically and chemically precipitated $CaCO_3$ from the water column. Accordingly, the Ölüdeniz sediment sequence is informative about whether the terrestrial clastic fraction increases or bio/chemical $CaCO_3$ precipitation from the water column decreases within tsunami-
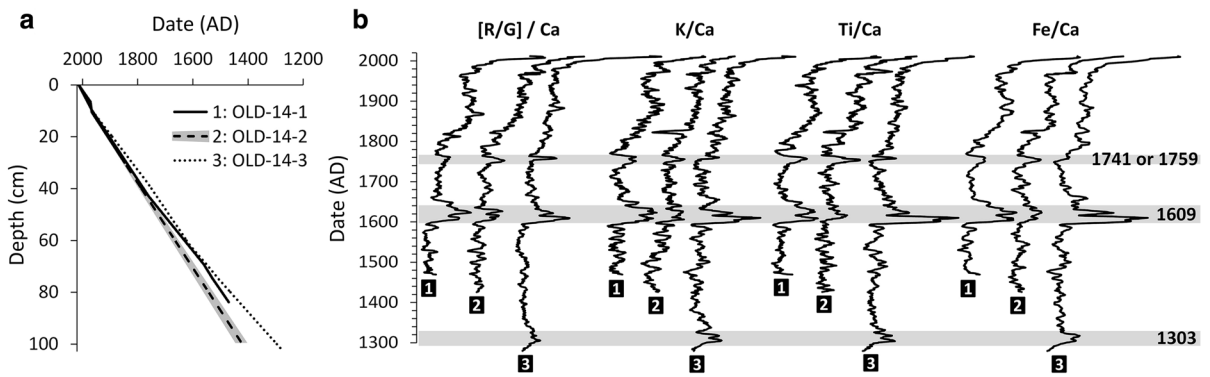
Fig. 6 a Age-depth models for OLD-14-1 and OLD-14-3 obtained by stratigraphic correlation with OLD-14-2. **b** Stratigraphic correlation between the three cores. OLD-14-3 reveals one more event (E3), which occurred in the early fourteenth century
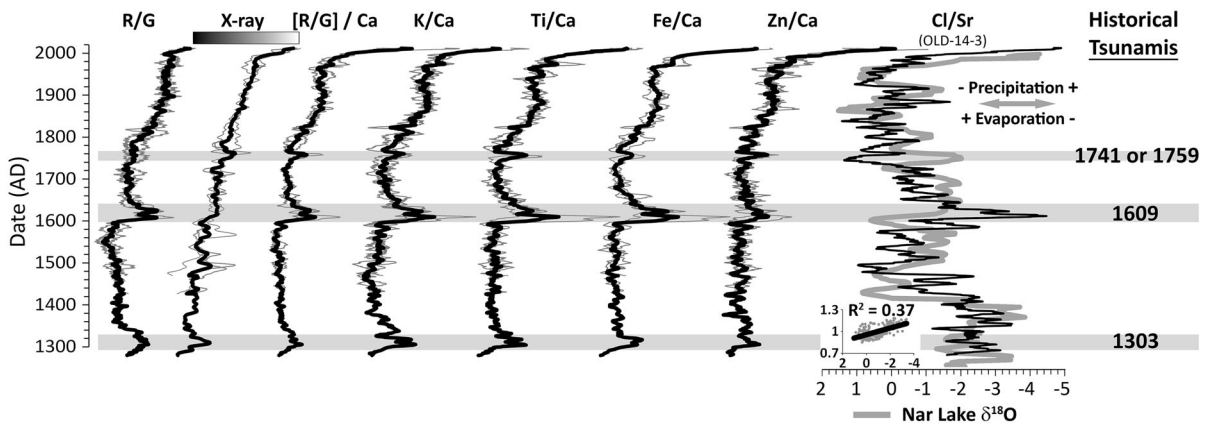

Fig. 7 Sediment variables from three cores (thin gray lines) overlapped by their average (thick black lines). The correlation between the Cl/Sr profile of OLD-14-3 and the varve-based

paleoclimate ($\delta^{18}O$) record from Nar Lake, is strong (r = 0.61), and supports the reliability of the age-depth models used

related deposits. Both cases are possible during marine overwash events into the lagoon. A tsunami wave would sweep significant amounts of clastic material from the Ölüdeniz beach and the sand spit, and transport it into the lagoon. Hence, these clastics would be deposited in the lagoon as an intercalation of material enriched in terrestrial-derived elements like Ti, Fe, K and Zn. During the relatively sudden deposition of these clastics, there would be no time for bio/chemical $CaCO_3$ precipitation from the water column, which would result in a Ca-depleted intercalation within the background sedimentation. Depletion of Ca is also supported by the [R/G]/Ca profile. This kind of dilution effect, caused by sudden sediment input during tsunamis, was also reported by Vött et al. (2009a) in the Sound of Lefkada (NW Greece), where the authors found extremely low amounts of pollen in

tsunami deposits. E1 is not clearly visible on the R/G profile, but when the R/G profile is divided by Ca, it becomes distinctly visible (Fig. 7). Grayscale profiles of the radiographic images, on the other hand, do not show any consistent anomalies related to tsunamis. Although E1 and E3 resulted in lighter tones in the radiographic images, implying less dense sediments, E2 is almost invisible.

Given that no macro plant remains were found in the sediments of the three cores, radiocarbon dating was not done. And although mollusk shells were encountered, dates on such material would be unreliable because of hard-water or reservoir effects in the lagoon. Instead, the chronology for the Ölüdeniz sediments was cross-checked by regional chronostratigraphic correlation. Nar Lake, which is located 500 km northeast of Ölüdeniz Lagoon (Fig. 1a),

provided a varve-based paleoclimate record (Jones et al. 2006). This record was used by Avşar et al. (2014) to cross-check the radiocarbon-based chronology from Göllüköy Lake, 350 km northeast of Nar Lake. Micro-XRF scanning results from Göllüköy sediments were correlated successfully with the $\delta^{18}O$ record of Nar Lake, and it was shown that chronostratigraphic correlation can be a useful tool for Anatolian sediment records. In the case of Ölüdeniz, the Chlorine (Cl)/Strontium (Sr) profile correlates reasonably with the $\delta^{18}O$ record of Nar Lake, especially in terms of fluctuations (Fig. 7). High precipitation and low evaporation periods in the Nar record are associated with high Cl/Sr values in the Ölüdeniz record. Although Sr intensity measured by scanners can originate from both mineral and seawater content of sediments, Chlorine (Cl) comes predominantly from seawater (Tjallingii et al. 2007). For this reason, the Cl/Sr profile can be used as an indicator of water content in sediments. High precipitation would lead to transport of coarser-grained sediments into the lagoon and result in higher water content, which would explain higher Cl/Sr values during high-precipitation periods.

The most prominent event (E2, from the AD 1609 tsunami) caused the largest deviation from the Nar Lake record. Very high Cl/Sr values associated with this event imply that the wave energy during the AD 1609 tsunami was much higher than during the other tsunamis, so it was able to transport much coarser grains into the lagoon, resulting in high water content. Accordingly, although the AD 1609 and 1741 tsunamis are both reported to have had intensities of 8 in the Rhodes Island region (Papadopoulos et al. 2014), the AD 1609 tsunami seems to have been stronger in and around the Ölüdeniz region compared to the AD 1741 tsunami. If the thickness and amplitude of anomalies presented in Fig. 7 are assumed to reflect intensity, the intensity of the AD 1303 tsunami seems to have been intermediate between the ones of AD 1609 and AD 1741. Historical sources report a tsunami in AD 1481, the intensity of which was 7 in the Rhodes Island region (Papadopoulos et al. 2014). Geological evidence for it was found in the Dalaman alluvial plain ("D" in Fig. 1, Papadopoulos et al. 2012), but this tsunami was not recorded in Ölüdeniz Lagoon. On the other hand, the AD 1609 event recorded in Ölüdeniz Lagoon is missing from the Dalaman record. Such comparisons

between geologic records illustrate how complex tsunami sediment deposition and preservation can be.

Increased terrigenous inputs into coastal lakes, as a consequence of tsunamis has been reported in few studies. Kempf et al. (2015, 2017) reported distinct tsunami-related magnetic susceptibility anomalies in coastal lakes of south-central Chile. They attributed high magnetic susceptibility values to delivery of greater amounts of terrigenous sediments to the lakes. Wagner et al. (2007) documented greater terrestrial input into coastal Loon Lake, East Greenland, during the Storegga tsunami. The authors characterized the tsunami deposit as having higher magnetic susceptibility values and lower total inorganic carbon (i.e. $CaCO_3$), similar to the Ca depletion in the Ölüdeniz record. In NW Java (Indonesia), van den Bergh et al. (2003) also reported magnetic susceptibility anomalies in shallow marine embayment sediments, caused by land-derived sediments transported into the bay by tsunami backwash. Unfortunately, there are no XRF scanning data in these studies that would enable us to make comparisons with geochemical traces of tsunamis.

Conclusions

Three sedimentary events (i.e. E1, E2 and E3) were detected in the sediment sequence from Ölüdeniz Lagoon and dated to approximately the early fourteenth century, early seventeenth century and middle eighteenth century. Temporal correlation between dates for these sedimentary events and historically recorded tsunamis in the eastern Mediterranean in AD 1303, 1609, and 1741 implies the events are tsunamigenic. The events are reddish-brown intercalations that show anomalies along their K/Ca, Ti/Ca, Fe/Ca and Zn/Ca profiles. The anomalies are attributed to sudden input of terrigenous sediment into the lagoon during tsunamis (i.e. K, Ti, Fe and Zn enrichment), as well as Ca depletion caused by a lack of time for bio/chemical precipitation of Ca from the water column during the sudden terrigenous sediment deposition. This study demonstrates that coastal lagoons and lakes are ideal places to detect well-preserved and continuous paleotsunami records, which are crucial to better assess tsunami hazards.

References

Alpar B, Ünlü S, Altınok Y, Özer N, Aksu A (2012) New approaches in assessment of tsunami deposits in Dalaman (SW Turkey). Nat Hazards 63:181–195

Avşar U, Hubert-Ferrari A, De Batist M, Lepoint G, Schmidt S, Fagel N (2014) Seismically-triggered organic-rich layers in recent sediments from Göllüköy Lake (North Anatolian Fault, Turkey). Quat Sci Rev 103:67–80

Baranes HE, Woodruff JD, Wallace DJ, Kanamaru K, Cook TL (2016) Sedimentological records of the C.E. 1707 Hoei Nankai Trough tsunami in the Bungo Channel, southwestern Japan. Nat Hazards 84:1185–1205

Barka A, Reilinger R (1997) Active tectonics of the Eastern Mediterranean region: deduced from GPS, neotectonic and seismicity data. Ann Geophys Italy 40:587–610

Bertrand S, Doner L, Akçer Ön S, Sancar U, Schudack U, Mischke S, Çağatay MN, Leroy SAG (2011) Sedimentary record of coseismic subsidence in Hersek coastal lagoon (Izmit Bay, Turkey) and the late Holocene activity of the North Anatolian Fault. Geochem Geophy Geosy 12:1–17

Borrero JC, Synolakis CE, Fritz H (2006) Northern Sumatra field survey after the December 2004 great Sumatra Earthquake and Indian Ocean Tsunami. Earthq Spectra 22:S93–S104

Bruins HJ, MacGillivray JA, Synolakis CE, Benjamini C, Keller J, Kisch HJ, Klügel A, van der Plicht J (2008) Geoarchaeological tsunami deposits at Palaikastro (Crete) and the Late Minoan IA eruption of Santorini. J Archaeol Sci 35:191–212

Chagué-Goff C (2010) Chemical signatures of palaeotsunamis: a forgotten proxy? Mar Geol 271:67–71

Chagué-Goff C, Schneider JL, Goff JR, Dominey-Howes D, Strotz L (2011) Expanding the proxy toolkit to help identify past events—lessons from the 2004 Indian Ocean Tsunami and the 2009 South Pacific Tsunami. Earth Sci Rev 107:107–122

Chagué-Goff C, Szczuciński W, Shinozaki T (2017) Applications of geochemistry in tsunami research: a review. Earth Sci Rev 165:203–244

Chandrasekharan H, Sarangi A, Nagarajan M, Singh VP, Rao DUM, Stalin P, Natarajan K, Chandrasekaran B, Anbazhagan S (2008) Variability of soil–water quality due to Tsunami-2004 in the coastal belt of Nagapattinam district, Tamilnadu. J Environ Manag 89:63–72

Clark K, Cochran U, Mazengarb C (2011) Holocene coastal evolution and evidence for paleotsunami from a tectonically stable region, Tasmania, Australia. Holocene 21:883–895

Dominey-Howes DTM, Cundy A, Croudace I (2000a) High energy marine flood deposits on Astypalaea Island, Greece: possible evidence for the AD 1956 southern Aegean tsunami. Mar Geol 163:303–315

Dominey-Howes DTM, Papadopoulos GA, Dawson AG (2000b) Geological and Historical Investigation of the 1650 Mt. Columbo Eruption and Tsunami, Aegean Sea, Greece. Nat Hazards 21:83–96

Donato SV, Reinhardt EG, Boyce JI, Pilarczyk JE, Jupp BP (2009) Particle-size distribution of inferred tsunami deposits in Sur Lagoon, Sultanate of Oman. Mar Geol 257:54–64

Dura T, Cisternas M, Horton BP, Ely LL, Nelson AR, Wesson RL, Pilarczyk JE (2015) Coastal evidence for Holocene subduction-zone earthquakes and tsunamis in central Chile. Quat Sci Rev 113:93–111

Fischer P, Finkler C, Röbke BR, Baika K, Hadler H, Willershäuser T, Rigakou D, Metallinou G, Vött A (2016) Impact of Holocene tsunamis detected in lagoonal environments on Corfu (Ionian Islands, Greece)—geomorphological, sedimentary and microfaunal evidence. Quat Int 401:4–16

Fuhrman DR, Eltard-Larsen B, Sumer BM, Baykal C, Dogulu N, Duha Metin A, Can Aydın D, Yalciner AC, Omira R, Lorenço N, Baptista MA (2015) D5.10—interaction of the tsunami with the seabed: implications for wind farms, aquaculture, coastal ecosystems and marine protected areas. ASTARTE Project Deliverable 5.10, 57 p. http://www.astarte-project.eu

Goff J, Lamarche G, Pelletier B, Chague-Goff C, Strotz L (2011) Predecessors to the 2009 South Pacific tsunami in the Wallis and Futuna archipelago. Earth Sci Rev 107:91–106

Goodman-Tchernov BN, Dey HW, Reinhardt EG, McCoy F, Mart Y (2009) Tsunami waves generated by the Santorini eruption reached Eastern Mediterranean shores. Geology 37:943–946

Goto K, Takahashi J, Oie T, Imamure F (2010) Remarkable bathymetric change in the nearshore zone by the 2004 Indian Ocean tsunami, Kirinda Harbor, Sri Lanka. Geomorphology 127:107–116

Graehl NA, Kelsey HM, Witter RC, Hemphill-Haley E, Engelhart SE (2015) Stratigraphic and microfossil evidence for a 4500-year history of Cascadia subduction zone earthquakes and tsunamis at Yaquina River estuary, Oregon, USA. Geol Soc Am Bull 127:211–226

Gutiérrez-Mas JM, Lopez-Arroyo J, Morales JA (2009) Recent marine lithofacies in Cadiz Bay (SW Spain) Sequences, processes and control factors. Sediment Geol 218:31–47

Hadler H, Willershäuser T, Ntageretzis K, Henning P, Vött A (2012) Catalogue entries and non-entries of earthquake and tsunami events in the Ionian Sea and the Gulf of Corinth (eastern Mediterranean, Greece) and their interpretation with regard to palaeotsunami research. In: Vött A, Venzke JF (eds) Jahrestagung des Arbeitskreises "Geographie der Meere und Küsten", vol 44. Bremer Beiträge zur Geographie und Raumplanung, Bremen, pp 1–15

Hoffmann N, Master D, Goodman-Tchernov B (2018) Possible tsunami inundation identified amongst 4–5th century BCE archaeological deposits at Tel Ashkelon, Israel. Mar Geol 396:150–159

ITIC (2018) International Tsunami Information Center. http://itic.ioc-unesco.org

Jackson KL, Eberli GP, Amelung F, McFadden MA, Moore AL, Rankey EC, Jayasena HAH (2014) Holocene Indian Ocean tsunami history in Sri Lanka. Geology 42:859–862

Jahns S (2005) The Holocene history of vegetation and settlement at the coastal site of Lake Voulkaria in Acarnania, western Greece. Veg Hist Archaeobot 14:55–66

Jones MD, Roberts NC, Leng MJ, Türkeş M (2006) A high-resolution late Holocene lake isotope record from Turkey and links to North Atlantic and monsoon climate. Geology 34:361–364

Kelsey HM, Nelson AR, Hemphill-Haley E, Witter RC (2005) Tsunami history of an Oregon coastal lake reveals a 4600 yr record of great earthquakes on the Cascadia subduction zone. Geol Soc Am Bull 117:1009–1032

Kempf P, Moernaut J, Van Daele M, Vermassen F, Vandoorne W, Pino M, Urrutia R, Schmidt S, Garrett E, De Batist M (2015) The sedimentary record of the 1960 tsunami in two coastal lakes on Isla de Chiloé, south central Chile. Sediment Geol 328:73–86

Kempf P, Moernaut J, Van Daele M, Vandoorne W, Pino M, Urrutia R, De Batist M (2017) Coastal lake sediments reveal 5500 years of tsunami history in south central Chile. Quat Sci Rev 161:99–116

Kitamura A, Fujiwara O, Shinohara K, Akaike S, Masuda T, Ogura K, Urano Y, Kobayashi K, Tamaki C, Mori H (2013) Identifying possible tsunami deposits on the Shizuoka Plain, Japan and their correlation with earthquake activity over the past 4000 years. Holocene 23:1684–1698

Mamo B, Strotz L, Dominey-Howes D (2009) Tsunami sediments and their foraminiferal assemblages. Earth Sci Rev 96:263–278

Mathes-Schmidt M, Schwarzbauer J, Papanikolaou I, Syberberg F, Thiele A, Wittkopp F, Reicherter K (2013) Geochemical and micropaleontological investigations of tsunamigenic layers along the Thracian Coast (Northern Aegean Sea, Greece). Z Geomorphol 57:005–027

May SM, Vött A, Brückner H, Smedile A (2012a) The Gyra washover fan in the Lefkada Lagoon, NW Greece—possible evidence of the 365 AD Crete earthquake and tsunami. Earth Planets Space 64:859–874

May SM, Vött A, Brückner H, Grapmayer R, Handl M, Wennrich V (2012b) The Lefkada barrier and beachrock system (NW Greece)—controls on coastal evolution and the significance of extreme wave events. Geomorphology 139–140:330–347

McLeod MK, Slavich PG, Irhas Y, Moore N, Rachman A, Ali N, Iskandar T, Hunt C, Caniago C (2010) Soil salinity in Aceh after the December 2004 Indian Ocean tsunami. Agric Water Manag 97:605–613

Minoura K, Imamura F, Kuran U, Nakamura T, Papadopoulos GA, Takahashi T, Yalçıner AC (2000) Discovery of Minoan tsunami deposits. Geology 28:59–62

Mischke S, Schudack U, Bertrand S, Leroy SAG (2012) Ostracods from a Marmara Sea lagoon (Turkey) as tsunami indicators. Quat Int 261:156–161

Morhange C, Marriner N, Pirazzoli PA (2006) Evidence of late-Holocene tsunami events in Lebanon. Z Geomorphol 146(Supp):81–95

Mori N, Takahashi T, Yasuda T, Yanagisawa H (2011) Survey of 2011 Tohoku earthquake tsunami inundation and run-up. Geophys Res Lett 38:1–6

Nanayama F, Satake K, Furukawa R, Shimokawa K, Atwater BF, Shigeno K, Yamaki S (2003) Unusually large earthquakes inferred from tsunami deposits along the Kuril trench. Nature 424:660–663

Nanayama F, Furukawa R, Kiyoyuki S, Makino A, Soeda Y, Igarashi Y (2007) Nine unusually large tsunami deposits from the past 4000 years at Kiritappu marsh along the southern Kuril Trench. Sediment Geol 200:275–294

Öğretmen N, Cosentino D, Gliozzi E, Cipollari P, Iadanza A, Yıldırım C (2015) Tsunami hazard in the Eastern Mediterranean: geological evidence from the Anatolian coastal area (Silifke, southern Turkey). Nat Hazards 79:1569–1589

Papadopoulos GA, Imamura F (2001) A proposal for a new tsunami intensity scale. In: Proceedings of the International Tsunami Symposium 2001, Seattle, pp 569–577

Papadopoulos GA, Minoura K, Imamura F, Kuran U, Yalçıner A, Fokaefs A, Takahashi T (2012) Geological evidence of tsunamis and earthquakes at the Eastern Hellenic Arc: correlation with historical seismicity in the eastern Mediterranean Sea. Res Geophys 2:90–99

Papadopoulos GA, Gràcia E, Urgeles R, Sallares V, De Martini PM, Pantosti D, González M, Yalciner AC, Mascle J, Sakellariou D, Salamon A, Tinti S, Karastathis V, Fokaefs A, Camerlenghi A, Novikova T, Papageorgiou A (2014) Historical and pre-historical tsunamis in the Mediterranean and its connected seas: geological signatures, generation mechanisms and coastal impacts. Mar Geol 354:81–109

Peterson CD, Carver GA, Cruikshank KM, Abramson HF, Garrison-Laney CE, Dengler LA (2011) Evaluation of the use of paleotsunami deposits to reconstruct inundation distance and runup heights associated with prehistoric inundation events, Crescent City, southern Cascadia margin. Earth Surf Proc Land 36:967–980

Pilarczyk JE, Reinhardt EG (2012) Testing foraminiferal taphonomy as a tsunami indicator in a shallow arid system lagoon: Sur, Sultanate of Oman. Mar Geol 295–298:128–136

Pirazzoli PA, Ausseil-Badie J, Giresse P, Hadjidakit E, Arnold M (1992) Historical environmental changes at Phalasarna harbour, West Crete. Geoarchaeology 7:371–392

Ramírez-Herrera MT, Lagos M, Hutchinson I, Kostoglodov V, Machain ML, Caballero M, Goguitchaichvili A, Aguilar B, Chagué-Goff C, Goff J, Ruiz-Fernández AC, Ortiz M, Nava H, Bautista F, Lopez GI, Quintana P (2012) Extreme wave deposits on the Pacific coast of Mexico: Tsunamis or storms?—a multi-proxy approach. Geomorphology 139–140:360–371

Razjigaeva NG, Ganzey LA, Grebennikova TA, Ivanova ED, Kharlamov AA, Kaistrenko VM, Arslanov KhA, Chernov SB (2014) The Tohoku Tsunami of 11 March 2011: the key event to understanding tsunami sedimentation on the coasts of closed bays of the Lesser Kuril Islands. Pure Appl Geophys 171:3307–3328

Röbke BR, Vött A (2017) The tsunami phenomenon. Prog Oceanogr 159:296–322

Ruiz F, Abad M, Cáceres LM, Vidal JR, Carretero MI, Pozo M, González-Regalado ML (2010) Ostracods as tsunami tracers in Holocene sequences. Quat Res 73:130–135

Salamon A, Rockwell T, Ward SN, Guidoboni E, Comastri A (2007) Tsunami hazard evaluation of the Eastern Mediterranean: historical analysis and selected modeling. Bull Seismol Soc Am 97:1–20

Sawai Y, Kamataki T, Shishikura M, Nasu H, Okamura Y, Satake K, Thomson KH, Matsumoto D, Fujii Y, Komatsubara J, Aung TT (2009) Aperiodic recurrence of geologically recorded tsunamis during the past 5500 years in eastern Hokkaido, Japan. J Geophys Res 114:B01319

Scheffers A, Scheffers S (2007) Tsunami deposits on the coastline of west Crete (Greece). Earth Planet Sci Lett 259:613–624

Shah-Hosseini M, Saleem A, Mahmoud AMA, Morhange C (2016) Coastal boulder deposits attesting to large wave impacts on the Mediterranean coast of Egypt. Nat Hazards 83:849–865

Smedile A, De Martini PM, Pantosti D, Bellucci L, Del Carlo P, Gasperini L, Pirrotta C, Polonia A, Boschi E (2011) Possible tsunami signatures from an integrated study in the Augusta Bay offshore (Eastern Sicily-Italy). Mar Geol 281:1–13

Stanley JD, Bernasconi MP (2006) Holocene Depositional Patterns and Evolution in Alexandria's Eastern Harbor, Egypt. J Coast Res 22:283–297

Tjallingii R, Röhl U, Kölling M, Bickert T (2007) Influence of the water content on X-ray fluorescence core-scanning measurements in soft marine sediments. Geochem Geophys Geosyst 8:1–12

Tyuleneva N, Braun Y, Katz T, Suchkov I, Goodman-Tchernov B (2018) A new chalcolithic-era tsunami event identified in the offshore sedimentary record of Jisr al-Zarka (Israel). Mar Geol 396:67–78

van den Bergh GD, Boer W, de Haas H, van Weering TJCE, van Wijhe R (2003) Shallow marine tsunami deposits in Teluk Banten (NW Java, Indonesia), generated by the 1883 Krakatau eruption. Mar Geol 197:13–34

Vött A, May M, Brückner H, Brockmüller S (2006) Sedimentary evidence of late Holocene tsunami events near Lefkada Island (NW Greece). Z Geomorphol (Suppl Vol) 146:139–172

Vött A, Brüeckner H, Brockmüeller S, Handl M, May SM, Gaki-Papanastassiou K, Herd R, Lang F, Maroukian H, Nelle O, Papanastassiou D (2009a) Traces of Holocene tsunamis across the Sound of Lefkada, NW Greece. Glob Planet Change 66:112–128

Vött A, Brückner H, May SM, Sakellariou D, Nelle O, Lang F, Kapsimalis V, Jahns S, Herd R, Handl M, Fountoulis I (2009b) The Lake Voulkaria (Akarnania, NW Greece) palaeoenvironmental archive—a sediment trap for multiple tsunami impact since the mid-Holocene. Z Geomorphol (Suppl Vol) 53(1):1–37

Vött A, Lang F, Brüeckner H, Gaki-Papanastassiou K, Maroukian H, Papanastassiou D, Giannikos A, Hadler H, Handl M, Ntageretzis K, Willershaeuser T, Zander A (2011) Sedimentological and geoarchaeological evidence of multiple tsunamigenic imprint on the Bay of Palairos-Pogonia (Akarnania, NW Greece). Quat Int 242:213–239

Vött A, Bruins HJ, Gawehn M, Goodman-Tchernov BN, De Martini PM, Kelletat D, Mastronuzzi G, Reicherter K, Röbke BR, Scheffers A, Willershäuser T, Avramidis P, Bellanova P, Costa PJM, Finkler C, Hadler H, Koster B, Lario J, Reinhardt E, Mathes-Schmidt M, Ntageretzis K, Pantosti D, Papanikolaou I, Sansò P, Scicchitano G, Smedile A, Szczuciński W (2018) Publicity waves based on manipulated geoscientific data suggesting climatic trigger for majority of tsunami findings in the Mediterranean—response to 'Tsunamis in the geological record: making waves with a cautionary tale from the Mediterranean' by Marriner et al. (2017). Z Geomorphol (Supp Vol) 1:2. https://doi.org/10.1127/zfg_suppl/2018/0547

Wagner B, Bennike O, Klug M, Cremer H (2007) First indication of Storegga tsunami deposits from East Greenland. J Quat Sci 22:321–325

Werner V, Baika K, Fischer P, Hadler H, Obrocki L, Willershäuser T, Tzigounaki A, Tsigkou A, Reicherter K, Papanikolaou I, Emde K, Vött A (2018) The sedimentary and geomorphological imprint of the AD 365 tsunami on the coasts of southwestern Crete (Greece)—examples from Sougia and Palaiochora. Quat Int 473:66–90

Whelan F, Kelletat D (2002) Geomorphic evidence and relative and absolute dating results for tsunami events on Cyprus. Sci Tsunami Hazard 20:3–18

Willershäuser T, Vött A, Hadler H, Ntageretzis N, Emde K, Brückner H (2015) Holocene palaeotsunami imprints in the stratigraphical record and the coastal geomorphology of the Gialova Lagoon near Pylos (southwestern Peloponnese, Greece). Z Geomorphol (Supp Vol) 59(4):215–252

Wilson R, Davenport C, Jaffe B (2012) Sediment scour and deposition within harbors in California (USA), caused by the March 11, 2011 Tohoku-oki tsunami. Sediment Geol 282:228–240

Yolsal S, Taymaz T, Yalçıner AC (2007) Understanding tsunamis, potential source regions and tsunami-prone mechanisms in the Eastern Mediterranean. In: Taymaz T et al (eds) The Geodynamics of the Aegean and Anatolia, vol 291. Geol Soc Spec Publ, London, pp 201–230